# Survey of the Excited State Dissociation of Gas-Phase Bromine Monochloride in the Visible–Near UV Wavelength Region

D. Zhang*

College of Science, Huazhong Agricultural University, Wuhan 430070, PR China

*(Received October 28, 2009)*

The spectroscopic transitions and photoabsorption/dissociation processes of bromine monochloride (BrCl) via several low-lying covalently bound electronic states and repulsive states have been investigated by performing electronic structure calculations and wave packet simulations of nuclear motion. The absorption spectra for 52-electron singlet systems are obtained by employing time-dependent propagation methods or the real-time propagation of the time-dependent Schrödinger equations in the adiabatically exact approximation. Based on the elastic scattering calculations, the results of angular distributions of the products of photodissociation of BrCl molecules are examined on two aspects: (1) the nature of the state that is prepared by excitation from a bound level into a continuum, and (2) under avoided crossing cases, the influences of nonadiabatic coupling processes on the fragmentation process are evaluated by virtue of a semiclassical Landau–Zener model, which treats an avoided crossing between two states of a given nature and evaluates a nonadiabatic effect relevant to the molecule during photodissociation. The model qualitatively reproduces the key aspects of the full processes related to the transfer of dissociating flux between states of $0^+$ symmetry, indicating that the proposed coupling scheme is generally correct.

PACS numbers: 31.15.Qg, 33.20.Kf, 31.50.Gh

## 1. Introduction

Reaction dynamics of photoinduced chemical reactions is an important topic in modern physical chemistry [1–4]. As a branch, the studies of photodissociation processes represent the milestone concepts of chemistry, which provide detailed insight into excited molecule interplay and bond cleavage [5–7]. The movement of an electron from the bond being broken to the bond being formed is induced by nuclear motion and may be thought of as an electronically nonadiabatic process. In that sense, the nonadiabatic coupling of electronic and nuclear motions lies at the heart of the photochemistry of excited molecules. Excited electronic states are quite common in nature, encountered, for example, in processes such as ignition, respiration, light absorption, and fluorescence. A thorough understanding of the excited state processes is essential for the possibility to actively intervene with and ultimately control the outcome of a chemical reaction [8–13]. In reality, the most challenging and revealing modern developments come from the measurement and interpretation of vector properties, determined by polarization dependent final state analysis. The interplay of coherent and incoherent channels, adiabatic and nonadiabatic paths, as revealed in angular distributions, correlated speed distributions, and fragment polarization, when combined with modern theory has been the path of recent progress.

The halogen containing molecules such as hydrogen halides, H–X (X = F, Cl, Br, I) provide excellent models to study intramolecular processes involving several potential energy surfaces. Though apparently simple, these molecules have proven to be an excellent test-bed both for technique refinement and for testing approximations inherent in the Born–Oppenheimer approximation. Wave packet motion in diatomic molecules represents the rudimentary model system where curve crossing manifests itself and thereby serves as a cornerstone for understanding limits to the reduced-dimensionality descriptions often used in multimode dynamics. Besides, halogen atoms and halogen-containing radicals have been realized as efficient chemical species for the destruction of stratospheric ozone. Thus, it is important to determine their photodynamic behavior for assessing their environmental impact. Therefore, these halogen molecules have received much experimental and theoretical attention and served as a paradigm for research into fundamental photodissociation processes in the visible and near UV wavelength range lately.

As compared with hydrogen halides, the photodissociation processes of interhalogen molecules, X–Y (X, Y = F, Cl, Br, I) have been less studied. The main reason is that a large number of Born–Oppenheimer electronic states correlating to the four possible atomic asymptotes for neutral $^2P_J$ ($J = 1/2$ or $3/2$) atoms and thus the pho-

* e-mail: dxiexidu@ymail.com

todissociation processes for these type of molecules are more complicated, because more electronic states may be involved to make multiple dissociation channels probable. For BrCl molecules or similar systems, the electronic properties and dissociation limit have been explored in detail [14–20]. The results indicate that at least 22 electronically excited states and the ground state correlate with $\mathrm{Br}\,(^2P) + \mathrm{Cl}\,(^2P)$ atoms.

Concerning the electronic spectra of BrCl, however, the lowest absorption band for this molecule is broad and featureless. In principle, the deconvolution of its continuous absorption spectrum within the range of 200–550 nm can be done as regards to excitations to only three or four electronically excited states. Such treatments, which assume that the total absorption can be decomposed into the requisite number of overlapping band envelopes, each of which can be parameterized in terms of a simple analytic function, have led to the well-known spectral assignments.

Molecular BrCl may undergo bond fission, upon excitation to the $A$-band ($\pi$ or $\pi^*$, $\sigma^*$) that comprise three overlapping states denoted as $A^3\Pi(1)$, $B^3\Pi(0^+)$ and $C^1\Pi(1)$ in the ascending order. The $A^3\Pi(1)$ and $C^1\Pi(1)$ correlate to the Cl fragment with a transition dipole moment perpendicular to the bond axis, whereas the $B^3\Pi(0^+)$ correlates to the Cl with the transition dipole moment aligned parallel to the Br–Cl bond. As reported, the formation of Cl and Cl$^*$ product is not a direct process. Although different population of different states is due to different dipole moments between the ground and the different excited states, the avoided crossing plays an important role in the branching processes by permitting rapid population transfer between the two adiabatic surfaces coupled by the seam of the crossing. Thus the energy partitioning and angular anisotropy of final products (Cl and Cl$^*$) have been the focus of the study. The consequences rely on the excitation wavelength and the nonadiabatic nature of the $A$-band photodissociation.

A recent study of the photodissociation of bromine monochloride over the wavelength of 320–570 nm provided the quantum yields of Cl and Cl$^*$, as well as the related anisotropy parameter [21]. Accordingly, the avoided crossing probabilities were predicted to rise gradually with the decrease of the wavelength. But the photolyzing wavelengths are away from the region of the avoided crossing such that the behavior of the nonadiabatic transition cannot be effectively compared with the case of hydrogen halides that these molecules should dissociate rapidly in the regime of 100–200 fs.

According to the one-dimensional Landau–Zener model [22], the heavier molecules lead to a slower velocity through the avoided crossing region such that the $B^3\Pi(0^+)$ state may have more probability to bifurcate in the crossing region of the diabatic $B$ and $D$ state potentials, while the later potential corresponds to the $D(0^+)-X^1\Sigma^+(0^+)$ transition. Opposed to symmetry--required intersections, which occur between two degenerate electronic excited states that belong to the same irreducible representation, the avoided crossing remains valid for $B$ and $D$ states in BrCl since the diabatic $D$ state possesses the same symmetry with the $B$ state.

It may occur that an ascending and a descending surface of the same symmetry approach the same value of the energy leading to an avoided crossing, the curves therefore repel each other. What happens at this point is of great interest in the research of nonadiabatic interaction in mutually coupled potential energy curves, because the interaction between the $B$ and $D$ state potentials at extended bond lengths controls the extent of the parallel contribution to the ground state dissociation yield. Regarding this question, BrCl photodissociation provides a unique opportunity to study the non-adiabatic interactions. Since both the chlorine and the bromine fragments have two spin–orbit states, there are four possible exit channels near the dissociation limit. Although a qualitative agreement is reached in the dynamic trend for the quantum yields of Cl and Cl$^*$, as well as the related anisotropy parameter, however, the spectroscopic studies and the consequent dissociation mechanism remain to be investigated in detail.

In supplement to the previous work, we study the photodissociation of bromine monochloride in a theoretical background, attempting to gain more detailed information. The branching processes of Cl and Cl$^*$ photofragments are explored by the semiclassical method directly in combination with the time-dependent density functional theory (TDDFT), and the Landau–Zener transition probability theory for the nonadiabatic crossing of energy level is applied in this system. The quantum yields and anisotropy parameters are thus determined during the process of the Br–Cl bond rupture, and the beta parameter is compared with the experimental value estimated from the Landau–Zener nonadiabatic transition model. The interaction between diabatic $B$ and $D$ state potentials is for the first time predicted that may be eventually compared with still nonexistent experimental results in this system and the intervening mechanism is discussed to unravel the dynamics features for the photodissociation of BrCl.

## 2. Numerical approach

In a photodissociation process, the molecule starts in a well defined initial state and ends up in a final scattering state. The initial bound state vibrational-rotational wave function provides a natural initial wave packet in this case. The key to performing a wave packet calculation is the propagation of the wave packet forward in time so as to solve the following time-dependent Schrödinger equation:

$$\mathrm{i}\hbar\frac{\partial|\,\Psi(x,t)\rangle}{\partial t} = H|\,\Psi(x,t)\rangle\,, \tag{1}$$

where $\Psi$ is a column vector of wave functions, $x$ are the coordinates of the particles and $H$ is the molecular Hamiltonian containing the kinetic energy of system and Coulomb interaction between all the electrons and nuclei.

The initial wave packets are constructed by multiplying the ground state vibrational wave function $\xi_\nu$ by the appropriate transition moment functions $\mu_j(R)$:

$$[\Psi(R,t=0)] = \begin{pmatrix} \Psi_1(R,t=0) = \mu_1(R)\xi_\nu \\ \Psi_2(R,t=0) = \mu_2(R)\xi_\nu \\ \vdots \\ \Psi_n(R,t=0) = \mu_n(R)\xi_\nu \end{pmatrix}, \quad (2)$$

where $[\Psi(R,t=0)]$ denotes an ensemble of the initial wave packet $\Psi_j(R,t=0)$ $(j=1,2,\ldots,n)$ formed on the $j$-th excited state in a matrix representation, $\mu_j(R)$ is the transition moment associating the $j$-th excited state with the ground state.

The Schrödinger equation is solved using the split-operator method which employs a symmetric splitting of the kinetic and potential energy operators to approximate the evolution operator

$$\begin{aligned} \Psi(R,t+\mathrm{d}t)\rangle &= \mathrm{e}^{-\mathrm{i}\,\mathrm{d}t\hat{H}/\hbar}\,\Psi(R,t) \\ &= \mathrm{e}^{-\mathrm{i}\,\hat{V}\,\mathrm{d}t/2\hbar}\,\mathrm{e}^{-\mathrm{i}\,\hat{T}\,\mathrm{d}t/\hbar}\,\mathrm{e}^{-\mathrm{i}\,\hat{V}\,\mathrm{d}t/2\hbar}\,\Psi(R,t) \\ &\quad + \mathrm{O}(\mathrm{d}t^3)\,, \end{aligned} \quad (3)$$

where $\mathrm{d}t$ is the increment in time. The action of the potential-energy operator is carried out in the coordinate space and that of the kinetic-energy operator in the momentum space, where it is diagonal.

In the time-dependent quantum-mechanical formalism, the total photoabsorption spectrum as a function of the photon energy $h\nu$ is given by the Fourier transform of the autocorrelation function

$$\sigma(\omega) = \frac{2\pi\omega}{3\hbar c}\int_{-\infty}^{\infty} \mathrm{d}t w(t) C(t)\,\mathrm{e}^{\mathrm{i}\,Et/\hbar}\,, \quad (4)$$

where $E = E_0 + h\omega$ is the total energy with $E_0$ being the energy of the initial rovibrational eigenstate and $C(t)$ is the autocorrelation function. A Hann window function $w(t) = 1 + \cos(\pi t/T)$ is included in Eq. (4), because we truncate the temporal integration limits to a finite range $[-T,T]$, where $T$ is the total propagation time. This prevents undesirable side bands in the absorption spectrum. The autocorrelation function is defined as the projection of the propagating wave function onto the initial state wave function at each time step

$$C(t) = \langle\,\Psi(t=0)|\,\Psi(t)\rangle\,. \quad (5)$$

To obtain the partial photodissociation cross-section, the wave packet at an analysis line $R = R_f$ is Fourier transformed from the time to the energy domain

$$A_j(E) = \frac{1}{2\pi}\int_0^{\infty} A_j(R_f,t)\exp(\mathrm{i}Et/\hbar)\,\mathrm{d}t \quad (6)$$

and the partial cross-section in channel $j$ is extracted according to

$$\sigma_j(\omega) = \frac{4\pi^3}{3c\varepsilon_0 m} k_j \omega |A_j(E)|^2, \quad (7)$$

where $m$ is the reduced mass of BrCl, $k_j = (1/\hbar)[2m(E - V(\infty)]^{1/2}$ is the wave vector in channel $j$, and $\varepsilon_0$ is the permittivity of free space. It can be deduced that the total cross-section in Eq. (4) is the sum of the partial cross-sections in Eq. (7), i.e.

$$\sigma_{\mathrm{tot}}(\omega) = \sum_j \sigma_j(\omega)\,. \quad (8)$$

The calculations are performed using equidistant grids for the internuclear coordinate. As the dissociating wave packets reach the asymptotic region, they must be attenuated by the negative complex absorbing potential. The coefficients ($M_{\mathrm{abs}}$) of absorbing potential are

$$\begin{aligned} &M_{\mathrm{abs}}(R) = 1.0, \quad \text{for} \quad R < R_{\mathrm{abs}}, \\ &M_{\mathrm{abs}}(R) = \exp(-\alpha_{\mathrm{opt}}\,\mathrm{d}t)\left(\frac{R - R_{\mathrm{abs}}}{R_{\mathrm{max}} - R_{\mathrm{abs}}}\right)^{3/2} \\ &\quad \text{for} \quad R_{\mathrm{abs}} < R < R_{\mathrm{max}}\,, \end{aligned} \quad (9)$$

where $R_{\mathrm{abs}}$ is the starting point of damping, $\alpha_{\mathrm{opt}}$ is an optimum factor for damping. Values of all parameters used in calculations are listed in Table I. The simulations of nuclear motion are performed by using the source code of FORTRAN language. In the computations of electronic structure, the occupied orbital space is divided into a set of inactive or closed-shell orbitals and a set of active orbitals. All inactive orbitals are doubly occupied in each Slater determinant. The active orbitals have varying occupations, and all possible Slater determinants (or CSFs) are taken into account which can be generated by distributing the $N_{\mathrm{act}} = N_{\mathrm{el}} - 2m_{\mathrm{closed}}$ electrons in all possible ways among the active orbitals, where $m_{\mathrm{closed}}$ is the number of closed-shell (inactive) orbitals, and $N_{\mathrm{el}}$ is the total number of electrons. Thus, it corresponds to a full configuration interaction in the active space. On this basis, the relevant 14 electrons are set as active, and the orbital selections are carried out at the restricted Hartree–Fock (RHF) level: (I) a minimal space $(2,2)$ based on a reduced highly occupied molecular orbital (HOMO) and lowly unoccupied molecular orbital (LUMO) occupation, involving only the valence orbitals and not accounting for correlation with other orbitals; (II) a quasi-minimal active space $(4,4)$ built by adding the (H−1)OMO and (L+1)UMO orbitals to the previous space; and (III) the largest possible formed by all the energetically close active valence $\pi$-orbitals, the

TABLE I

Values, with units, of the numerical parameters used in the numerical calculations for BrCl.

| | | | |
|---|---|---|---|
| Atomic masses | $m(^{35.45}\mathrm{Cl})$ | 35.453 | amu |
| | $m(^{79.90}\mathrm{Br})$ | 79.904 | amu |
| Range of grid | $R_{\mathrm{min}}$, $R_{\mathrm{max}}$ | 3.48–14.72 | $a_0$ |
| Number of grid points | | 4096 | |
| Position of analysis line | $R_f$ | 12.72 | $a_0$ |
| Time step | $\mathrm{d}t$ | 0.483776 | fs |
| Number of time steps | | 8192 | |
| Start of absorbing region | $R_{\mathrm{abs}}$ | 13.22 | $a_0$ |
| Cubic damping factor | $\alpha_{\mathrm{opt}}$ | 0.015 | $E_h$ |

(14, 10) active space. The extended molecular orbitals of the ($[^2\Pi_{1/2}]5s\sigma$) Rydberg states required use of the standard aug-cc-pVDZ basis set. Practical active spaces consisted of 14 electrons occupying the usual valence orbitals, $(10\sigma)(11\sigma)(12\sigma)(5\pi)(6\pi)(13\sigma)$, to which 2 extra $\sigma$ orbitals are added in order to describe the lowest Rydberg orbitals of interest.

## 3. Results and discussion

Describing the electronic states of diatomic molecules, one should consider the $(+/-)$ symmetry symbol, related to the reflection with respect to the plane containing the main molecular axis, for both the $\Sigma$ states and $\sigma$ orbitals which are (de)populated for the considered transition to the given state. The potential energy curves for the $X^1\Sigma(0^+)$, $A^3\Pi(1)$, $B^3\Pi(0^+)$, $C^1\Pi(1)$ and $D^3\Sigma^-(0^+)$ states in the energy ascending order are shown in Fig. 1 as a function of internuclear distance. These curves can be cursorily divided into two types of potential curves.

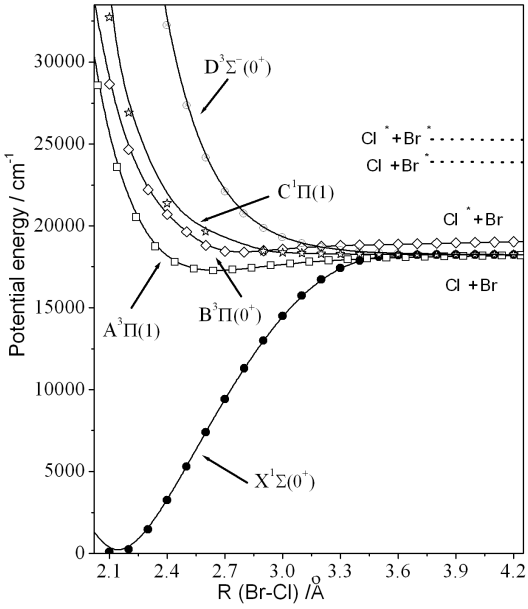


Fig. 1. The interaction potentials of bromine monochloride along the Cl–Br bond elongation coordinate at linear geometry, and various dissociation channels.

The first kind is those having shallow potential walls or having bound properties. The second type simply belongs to the repulsive curves. Among them, the $X^1\Sigma^+$ $(\Omega=0)$, $A^3\Pi_1$ $(\Omega=1)$, $C^1\Pi_1$ $(\Omega=1)$ and $D^3\Sigma^-$ $(\Omega=0)$ states asymptotically correlate to the ground state Cl($j=3/2$)+Br limit, whereas the $B^3\Pi_{0+}$ $(\Omega=0)$ state correlates with the excited state Cl*($j=1/2$)+Br dissociation limit.

In the case of the diatomic molecule represented here, the photodissociation process can be divided into two stages conceptually [23]. During the first stage the bound molecule absorbs a photon and is promoted to an excited state. This is generally an excited electronic state, but can be a highly excited vibrational state in the ground electronic state. In the second stage, the molecule enters the exit channel and dissociates into the products. When the molecule is promoted to an electronic state which has a purely repulsive potential energy surface (PES), it undergoes very rapid dissociation, often in less than one vibrational period. This is called direct dissociation. However, the dissociation of the excited molecule can be retarded, taking place over many vibrational periods. This is called indirect dissociation, or predissociation, and has been divided into three different categories.

According to the topology of potential energy surfaces (PESs), the fragmentation mechanism should arise from the electronic predissociation (Herzberg type I). In this case, the PES of the electronically excited state is not dissociative at the given energy, and in order to dissociate the molecule must undergo a nonadiabatic transition to a second dissociative electronic state. This involves the coupling of nuclear and electronic motion and therefore leads to a breakdown of the Born–Oppenheimer (BO) approximation. There are two main types of electronic predissociation. In the first case, there is only a very small coupling, and no actual crossing, between two different electronic states, and the transition between the two is driven by the very high density of vibrational states on the second electronic state. This is called internal conversion for spin-allowed processes, and intersystem crossing for spin-forbidden processes. In the second case, the transition between the electronic states is driven by strong coupling. This coupling can be vibronic (vibrational--electronic) in nature, e.g., for the Renner–Teller and Jahn–Teller effects [24], or purely electronic, as in the case of an avoided crossing.

As seen from Fig. 1, the diabatic curves correlating to final products split into two at large $R$. In the time domain picture, it means that the wave packet moves through the crossing region and splits into two smaller wave packets which can interfere with each other. This splitting is mainly responsible for the atom exchange process. With reference to Fig. 1, the initial state is a diabatic $B$-state wave packet which splits into two at the crossing region. A fraction will dissociate (adiabatic behavior) to Cl+Br products while the rest hops (diabatic behavior) to the upper adiabatic curve and continues out to the outer turning point. These two wave packets can be coupled by the curve crossing and thereby as they hop they will interfere with each other. This effect is expected to depend sensitively on coupling strength.

In the region of $E_h \approx 0.0852$ a.u. and $R \approx 6.05a_0$, a minimal energy crossing point exists, which results in a coupling of the quasi-bounding $B$ state with the repulsive states $D$. The effect originates from the intersecting located between the two involved adiabatic potential curves, which is in accord with the observation of the low resolution absorption spectrum of BrCl. The $X^1\Sigma_0^+$ electronic ground state of BrCl is characterized mainly by the closed-shell configuration $\sigma^2\pi^4\pi^{*4}\sigma^{*0}$. One excited con-

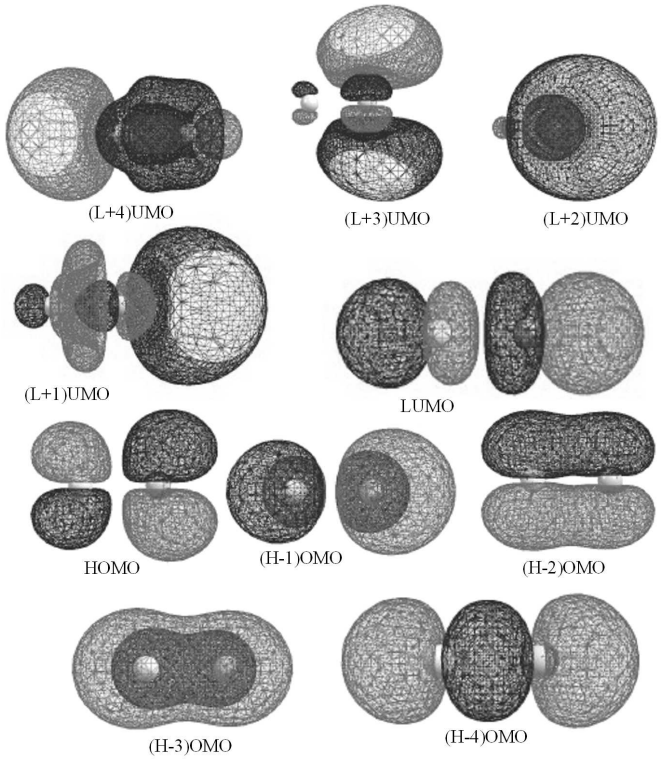


Fig. 2. Contour plots (from top to bottom) of the lowest unoccupied molecular orbital and highest occupied molecular orbitals (see Table II for their symmetry label) at the RHF ground state optimized geometry.

figuration, $\sigma^2\pi^4\pi^{*2}\sigma^{*2}$, having the $^3\Pi_{0+}$ symmetry, is dissociative [the $D(0^+)$ state] and correlates with ground Br+Cl($^2P_{3/2}$) channel. Another excited configuration, $\sigma^2\pi^4\pi^{*3}\sigma^{*1}$, also with $^3\Pi_{0+}$ symmetry, is bound (the $B$ state) and correlates to the Br+Cl$^*$($^2P_{1/2}$) channel. In the region of intersystem crossing, where the above two states become degenerate, the nonadiabatic transition can ultimately convert the photon energy into a non-statistical distribution of quantum flux. Due to the similar symmetry ($\Omega = 0^+$) of $B$ and $D$ electronic states, the avoided crossing is naturally formed between them. As will be discussed below, the avoided crossing plays a very important role in electronically nonadiabatic transitions.

For BrCl system, a systematic analysis of the excitations in a molecular approach like our current TDDFT computations is necessary, in particular, for polyatomic molecules for which the excited states are in a quasi-continuum. Each peak of the absorption spectra involves several molecular excitations with non-equivalent weights; an analysis based on the orbitals is therefore relevant. Following this, we have chosen to characterize the excitations by the charge density difference between the excited and the ground states for the main transitions (see Fig. 2). Blue (or dark) regions correspond to depletion of the electron density during the transition, while light colored (or violet) regions correspond to an increase of the electron density. Since any transition is a combination of many excitations among which the program used for calculations shows one or few excitations with the biggest contribution although this is a little approximation.

The description of the symmetry of the orbitals in Fig. 2 is the same, then it is seen in the pictures. As can be recognized, we show the relevant molecular orbitals that participate in the course of dissociation, which correlate to the low lying excited states of BrCl and contain the five HOMO and the five LUMO with their related bonding nature.

The positions of chlorine and bromine nuclei are indicated as bond direction, which is defined as $Z$-axis for the convenience of marking the valence $\pi$-orbitals. The MOs considered here are those that are relevant in Cl–Br cleavage of the BrCl molecule. In the atomic orbital (AO) approximation [25], if we are neglecting the polarity, the $^{3,1}\Pi$ configuration of mixed halogen such as BrCl should be $\sigma_{\mathrm{Cl}}\pi^4_{\mathrm{Cl}}\pi^2_{\mathrm{Br}}\sigma^3_{\mathrm{Br}}$ or $\sigma_{\mathrm{Br}}\pi^4_{\mathrm{Br}}\pi^2_{\mathrm{Cl}}\sigma^3_{\mathrm{Cl}}$. The MOs can be viewed as linear combination of AOs, thus the bonding orbitals can be written as $\sigma = c_1(3p\sigma_{\mathrm{Cl}}) + c_2(4p\sigma_{\mathrm{Br}})$, $\pi = c_3(3p\pi_{\mathrm{Cl}}) + c_4(4p\pi_{\mathrm{Br}})$; the anti-bonding orbitals can be written as $\sigma^* = c^*_1(4p\sigma_{\mathrm{Br}}) - c^*_2(3p\sigma_{\mathrm{Cl}})$, $\pi^* = c^*_3(4p\pi_{\mathrm{Br}}) - c^*_4(3p\pi_{\mathrm{Cl}})$. Here $c_1 > c_2$, $c_3 > c_4$, since chlorine is more electronegative than bromine. Apparently in the picture, the bonding $\pi$ or anti-bonding $\pi^*$ orbitals of the system, which are the five energetically highest occupied MOs, constitute the main source for the formation of the low-lying excited states.

Table II summarizes the low-lying excitations of the parent BrCl molecule. According to the computations, in both states, the transition from HOMO to LUMO ($25, 26 \rightarrow 27$) is found to dominate the absorption and transition is essentially a promotion of an electron from the bonding or anti-bonding $\pi$ orbital to the anti-bonding $\sigma$ orbital. During this process the partially bonding $\pi$(HOMO-2) orbital of the ground state may participate and give rise to the bonding $\pi$(HOMO-2) and anti-bonding $\pi$(HOMO) orbitals of the excited state. Because the excitation energies for the $22 \rightarrow 27$ transition lies very close to the Rydberg transition, the visible–near UV spectrum band can be ascribed largely to the transitions from HOMO-1 or HOMO orbitals to the first lowest unoccupied molecular orbital, namely, the front virtual orbital LUMO.

Figure 3 shows the extinction spectrum derived via the exact method of wave packet propagation, which is generated by projecting the ground state wave function onto the upper potential curves from which it is projected onto the energy axis. The width is related to the width of the wave function in the potential well, $X^1\Sigma^+_0$, and the slope of the upper potential energy curves. In fact, the molecule is vertically excited into the excited electronic state (the Franck–Condon principle) creating a population far from thermal equilibrium.

TABLE II

Details of the RHF orbitals employed to select the active spaces and their character, electric dipole moments $\mu_0$ (in $ea_0$) at equilibrium geometry.

| Assignments | $\mu_0$ $[ea_0]$ | Wave function important configuration | Orbital symmetries | Product atom correlation |
|---|---|---|---|---|
| $A^3\Pi(1)$ | 0.236 | $0.40461[(\mathrm{H}{-}1)^1 \to (\mathrm{L})^1] + 0.66618[(\mathrm{H})^1 \to (\mathrm{L})^1]$ | $\pi$; $\sigma^*$ | $\left\vert \frac{1}{2}\frac{1}{2}; \frac{3}{2}\frac{1}{2}\right\rangle$ |
| $B^3\Pi(0^+)$ | 0.514 | $0.66618[(\mathrm{H}{-}1)^1 \to (\mathrm{L})^1] - 0.40461[(\mathrm{H})^1 \to (\mathrm{L})^1]$ | $\pi$; $\sigma^*$ | $\frac{1}{\sqrt{2}}\left[\left\vert \frac{1}{2}\frac{1}{2}; \frac{1}{2}\frac{-1}{2}\right\rangle + \left\vert \frac{1}{2}\frac{-1}{2}; \frac{1}{2}\frac{1}{2}\right\rangle\right]$ |
| $C^1\Pi(1)$ | 1.041 | $0.63384[(\mathrm{H}{-}1)^1 \to (\mathrm{L})^1] + 0.16310[(\mathrm{H})^1 \to (\mathrm{L})^1]$ | $\pi$; $\sigma^*$ | $\left\vert \frac{1}{2}\frac{-1}{2}; \frac{3}{2}\frac{3}{2}\right\rangle$ |
| $D^3\Sigma^-(0^+)$ | 0.0 | $0.79210[(\mathrm{H}{-}4)^1 \to (\mathrm{L})^1] - 0.14408[(\mathrm{H}{-}1)^1 \to (\mathrm{L}{+}1)^1]$ | $\sigma$, $\pi$; $\sigma^*$ | $\left\vert \frac{1}{2}\frac{1}{2}; \frac{1}{2}\frac{1}{2}\right\rangle$ |

Recasting this qualitative picture in the theoretical framework of quantum dynamics, the intial excitation will prepare a nonstationary nuclear wave packet (WP). The time-evolution of the WP has an approximate classical representation in terms of a set of trajectories released on the excited state PES, whose initial positions and velocities "sample" the probability density of the quantum state. As is shown, the computed results of the partial extinction coefficient $\sigma$ (units: $\mathrm{mol}^{-1}$ L $\mathrm{cm}^{-1}$) to the $A$, $B$, and $C$ states reflect their relative weight in the initial population. For comparison the experimental spectrum of gas phase BrCl recorded over the wavelength range 220–500 nm ($25 \pm 2\,^{\circ}\mathrm{C}$) of Seery and Britton [26] is shown in the graph. One can discern that the $A$ band absorption continuum is obviously dominated by the allowed $C^1\Pi(1) \leftarrow X^1\Sigma(0^+)$ transition. The second allowed transition, $B^3\Pi(0^+) \leftarrow X^1\Sigma(0^+)$, is nearly 3.2 times weaker at its maximum. The corresponding partial absorption spectra are strongly shifted with respect to each other, so that absorption at energies below 21800.7 $\mathrm{cm}^{-1}$ is caused primarily by the $B \leftarrow X$ excitation. Transitions to the last states, $A^3\Pi(1)$, are slightly weaker, with its absorption curve placed under the $B \leftarrow X$ one. Here the photoexcitation to the higher $D^3\Sigma^-(0^+)$ state requires much more energy in the Franck–Condon region, which is unable to be accomplished directly via visible or near-UV photon. Thus, initial excitation to the $D^3\Sigma^-(0^+)$ state is discounted in our simulation.

In a photodissociation process, angular distribution $I(v,\theta)$ of the fragment is obtained by integrating the reconstructed three-dimensional spatial distribution over a proper range of speed $v$ at each angle $\theta$. Commonly, the angular distribution can then be expressed in an expansion of orthogonal Legendre polynomials [27]:

$$I(v,\theta) \propto \left(\frac{1}{4\pi}\right) f(v)\big[1 + \beta_2 P_2(\cos\theta) + \gamma_4 P_4(\cos\theta) + \xi_6 P_6(\cos\theta)\big]. \quad (10)$$

The parameter $\beta_2$ contains information on photofragment density. The parameters $\gamma_4$ and $\xi_6$ reflect the photofragment alignment. For a two-atom system, the modulation in the photofragment density is neglectable [28] and the velocity can be correlated with a molecular bond direction. On this occasion, the parameters $\gamma_4$ and $\xi_6$ in Eq. (10) vanish, and the spatial recoil distribution of fragments can be described by the anisotropy parameter $\beta$, according to the formula $I(v,\theta) = [1 + \beta P_2(\cos\theta)]/4\pi$, which reflects the dissociation dynamics and the symmetry of the potential energy surfaces involved.

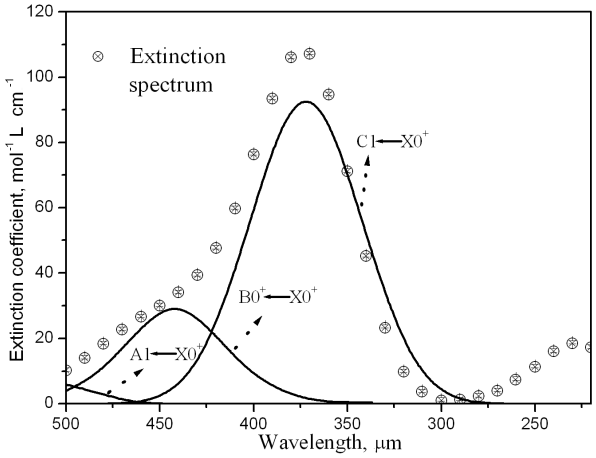


Fig. 3. Correlation between the photolysis wavelengths and the extinction coefficients. Open circles with error bars — experimental data from Ref. [26]; solid lines — numerical results.

More recently, state selected anisotropy parameters were obtained from a velocity map imaging technique for state selected fragments detected by REMPI. Aside from the direct excitation of $A^3\Pi_1$ and $C^1\Pi_1$ ($\Omega = 1$) states, the Cl channel with a positive $\beta(\mathrm{Cl})$ indicates the population transfers that significant contributions coming from the $B^3\Pi(0^+) \to D^3\Sigma^-(0^+)$ nonadiabatic transition cannot be completely neglected. The direction contribution in the Cl channel is considered to have a perpendicular character ($\beta = -1$), whereas the nonadiabatic contribution remains the same anisotropy as the $\mathrm{Cl}^*$ channel. Therefore, the $\beta(\mathrm{Cl})$ value may be resolved into the relative contributions of the parallel and perpendicular components by the formula [29, 30]:

$$\beta(\mathrm{Cl}) = a\beta_{\parallel} + b\beta_{\perp} = a\beta(\mathrm{Cl}^*) + b(-1)\,, \quad (11)$$

where $a$ and $b$, having a sum equal to unity, denote the fractions of nonadiabatic and direct-excitation contributions in the Cl product channel. The avoided crossing

probability, $P_{\rm ac}$, between the $B$ and $D$ states can be evaluated by the following equation:

$$P_{\rm ac} = \frac{a[1 - \Phi(\mathrm{Cl}^*)]}{\Phi(\mathrm{Cl}^*) + a[1 - \Phi(\mathrm{Cl}^*)]} \,. \tag{12}$$

Given the experimental data of $\beta(\mathrm{Cl})$, $\beta(\mathrm{Cl}^*)$ and quantum yield $\Phi(\mathrm{Cl}^*)$, $P_{\rm ac}$ may be determined at various wavelengths.

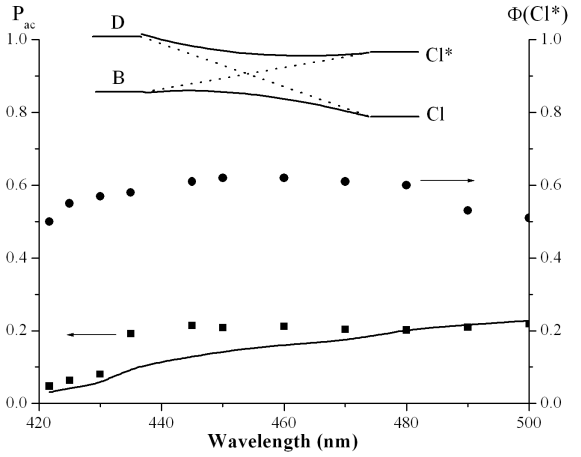


Fig. 4. The probability of avoided crossing and quantum yield of the $\mathrm{Cl}^*$ channel as a function of the dissociation wavelength. • denote the data of $\Phi(\mathrm{Cl}^*)$ adopted from Ref. [21], and ■ denote the $P_{\rm ac}$ inferred from the experimental findings. The solid curve is obtained from the present work, which is expected by the Landau–Zener model and assuming the coupling force between the $B$ and $D$ states is 90 $\mathrm{cm}^{-1}$.

Figure 4 shows the avoided crossing probability as a function of the excitation wavelength from 421.7 to 500 nm, which are determined according to the experimental data of Ref. [21]. The wavelength dependence of $\Phi(\mathrm{Cl}^*)$ is also shown in the graph. Let us note that the data at 435/445 nm may carry a slight uncertainty, because the selected wavelengths in this pair are far from each other. As is said before, photoexcitation at energies just above the first dissociation threshold can result in population of both the $A^3\Pi_1$ and $B^3\Pi(0^+)$ states of BrCl. The former state has a potential minimum and correlates adiabatically with ground state products. The $B$ state also displays a potential minimum but, in contrast, correlates diabatically with the spin–orbit excited products $\mathrm{Cl}^*$. As we discuss later, the $B$ state is subject to an avoided crossing (with the so-called $D$ state, of $0^+$ symmetry) at extended bond lengths, with the result that $B$ state molecules prepared by photon absorption from the ground state can follow an adiabatic pathway to ground state Cl products. This adiabatic pathway involves passage over a (small) energy barrier, the magnitude of which is sufficient to block dissociation.

When only two potential energy curves with an avoided crossing are involved, if the kinetic energy near the interaction region is small, the dissociation will proceed adiabatically, i.e., the molecule stays on the initially prepared adiabatic curve throughout the dissociation. For significantly higher kinetic energy, the dissociation can proceed diabatically and the molecule jumps to the other potential energy curve. As photodissociation occurs in a closer distance to the Landau–Zener type crossing point, the nonadiabatic transition probability ($p$) is expected to increase since the probability of avoided crossing is inversely proportional to the speed of the nuclei. The avoided crossing may be alternatively estimated by evoking a standard one-dimensional Landau–Zener theory as expressed by [31]:

$$p = 1 - \exp(-2\pi A^2/\hbar B u_\perp) \,, \tag{13}$$

where $u_\perp$ is the component of nuclear velocity which is perpendicular to the avoided crossing seam, $A = V_{B-D}$ and $B = |\mathrm{d}V_D/\mathrm{d}R - \mathrm{d}V_{\rm B}/\mathrm{d}R|$, here $A$ and $B$ were both evaluated at the avoided crossing, where $V_{B-D}$ represents the coupling strength between $B$ and $D$ states. Through this semiclassical multistate approach, the nonadiabatic steps can be treated by method of one-dimensional mean-field or surface hopping type. According to the analytical function of $B$ and $D$ state, the slopes of these two state potentials at the avoided crossing are 695.8 $\mathrm{cm}^{-1}$ $\mathrm{Å}^{-1}$, –2423.9 $\mathrm{cm}^{-1}$ $\mathrm{Å}^{-1}$ respectively, and then the difference in gradients between the above potentials or parameter $B$ is obtained to be 3119.7 $\mathrm{cm}^{-1}$ $\mathrm{Å}^{-1}$.

Given that the reliable avoided crossing point lies at $6.047a_0$ ($a_0 = 0.0529177$ nm is the Bohr radius), the interaction potential $V_{B-D}$ is assumed to be variable at this place (in the long range domain, weak interatomic interaction produces slow motion), $p$ may be readily estimated. In the simulation, the coupling strength or parameter $A$ may be in need of some modification. We began our prediction using an $R$-independent coupling strength, since the coupling term linking the diabatic $B$ and $D$ states cannot be viewed as a large perturbation compared with the asymptotic separation of the $B$ and $D$ state potentials. The choice of parameter $A$ is relevant to the simulation of the available data that were inferred from experiment, and so $A$ is set as adjustable to produce an acceptable fit with experimental findings.

Figure 4 shows the theoretical results of $P_{\rm ac}$ with its frequency dependence, which assuming the coupling strength $V_{B-D}$ are varied in the range of 60–120 $\mathrm{cm}^{-1}$, and the analysis is made following photolysis at wavelengths $\lambda$ = 421.7–500 nm. It could be found that a best-fit coupling matrix element is derived as $V_{B-D}$ = 90 $\mathrm{cm}^{-1}$, which successfully reproduces most of the observed phenomena within the error limit. The results reveal that the avoided crossing probability increases gradually in the early stage and then rises up dramatically with the increased wavelength. The abrupt increase of the perpendicular character of $\mathrm{Cl}(^2P_{3/2})$ suggests that the avoided crossing between the $B$ and $D$ states may be around 490 nm.

When the dissociation wavelength is tuned to pass the region of avoided crossing, $P_{\rm ac}$ increases only by $< 4.29\%$, suggesting that these two curves may cross almost parallel in the exit channel, regarding the description of

diabatic representation. Unfortunately, no significant signals of the $Cl^*/Cl$ pairs may be obtained when the photolyzing wavelength exceeds 490 nm. On the other hand, $\Phi(Cl^*)$ increases with the wavelength and then drops slightly after passing the region of avoided crossing. Increasing the $B \rightarrow D$ adiabatic transition should bring about the decrease of $\Phi(Cl^*)$.

As shown in Fig. 4, the probabilities of avoided crossing predicted in this work behave similarly as those observed in the case of BrCl but are slightly deviated at the regime of intermediate photolyzing wavelength. The $P_{ac}$ value is expected to increase as the nucleus becomes massive and the subsequent moving speed through the Landau–Zener crossing region becomes slower.

As stated above, the photodissociation process is thus anticipated to involve coupling primarily between the Br–Cl internal coordinate and the vibrational mode [32]. The nonadiabatic transition is substantially affected by the coupling strength between avoided crossing curves. The one-dimensional Landau–Zener theory indicates that a stronger coupling between two avoided crossing states may result in a larger adiabatic curve splitting and the subsequent avoided crossing probability, $P_{ac}$. Although the photodissociation of bromine monochloride does not involve the multidimensional character, a stronger coupling strength may analogously result in a larger $P_{ac}$. If we consider a simple limiting case in which the crossing between diabatic $0^+$ states is only weakly avoided, then most of the dissociating flux on the $B$ state will then follow the diabatic pathway to yield $Cl^*$.

The dissociation dynamics can be treated as occurring via excitation to the $A$ and $B$ states, with transfer of flux between these two potentials at short internuclear separation, followed by evolution to atomic products corresponding to channels associated with $\Omega = 1$ and $\Omega = 0$ diabatic curves, respectively. On this occasion, the nonlimiting experimental values of $\beta(Cl)$ and $\beta(Cl^*)$ can be easily explained in the limit of weak interaction of the two $0^+$ states, with a rotation-induced crossing between $B$ and $A$ state potentials. On the other hand, if the crossing between the $B(0^+)$ state and the higher-lying $D(0^+)$ state is strongly avoided, then the likely origin of reduced magnitude anisotropy parameters may be a consequence of a rotational coupling at small internuclear separation, an adiabatic evolution of dissociating flux through the avoided crossing (giving both parallel and perpendicular components to the Cl+Br asymptote), and a substantial flux transfer to one or more states correlating to $Cl^*$+Br. In reality, the coupling strength is concluded to be $\approx 90$ cm$^{-1}$, which represents the interesting case of intermediate coupling: a complete failure of the Born–Oppenheimer approximation where the wave packet evolution cannot be described by either the adiabatic (strong coupling) or diabatic (weak coupling) approximation. In this sense, the BrCl photodissociation should tend to have a larger nonadiabatic transition rate, however, the probability of avoided crossing will increase as the speed of nucleus becomes slower, which depends on the excitation wavelength during the course of fragmentation.

## 4. Conclusion

The photodissociation dynamics of bromine monochloride over the wavelength range of 388–500 nm was investigated. As expected, the Br+Cl channel, originating from the $A$ or $C$ state alone, is accompanied by the predissociation from $B$ state, which contributed by direct excitation and transition arising from the avoided crossing. The avoided crossing probability rises steadily around the region of intersystem crossing, but remains almost constant after passing through the intersystem crossing. The $B$ and $D$ states in the exit region are thus expected to cross almost parallel along the dissociation coordinate. Employing the classical Landau–Zener theory, the coupling strength between the above two states of $0^+$ symmetry is estimated to be $\approx 90$ cm$^{-1}$, as in the case of intermediate coupling, by the dynamical effect due to the advent of avoided crossing. On this occasion, a transition induced by the coupling force allows a part of dissociation flux originating from $B$ state to reach the Br+Cl channel, the outcome being a more isotropic distribution of low-velocity fragments produced at the longer excitation wavelength.

## Acknowledgments

This work was supported by Huazhong Agricultural University Scientific & Technological Self-innovation Foundation (2009QC016).

## References

[1] D.K. Belashchenko, O.I. Ostrovskii, *Russ. J. Phys. Chem. A* **82**, 364 (2008).

[2] D. Zhang, *Polish J. Chem.* **83**, 2009 (2009).

[3] D. Zhang, *Chem. Phys.* **353**, 87 (2008).

[4] G.E. Busch, R.T. Mahoney, R.I. Morse, K.R. Wilson, *J. Chem. Phys.* **51**, 837 (1969).

[5] D. Zhang, A. Abdel-Hafiez, B. Zhang, *Chem. Phys. Lett.* **428**, 49 (2006).

[6] Y. Matsumi, M. Kawasaki, T. Sato, T. Arikawa, *Chem. Phys. Lett.* **155**, 486 (1989).

[7] D. Zhang, *Russ. J. Phys. Chem. A* **82**, 2299 (2008).

[8] Y. Matsumi, K. Tonokura, M. Kawasaki, *J. Chem. Phys.* **97**, 1065 (1992).

[9] R.N. Zare, *Mol. Photochem.* **4**, 1 (1972).

[10] D. Zhang, A. Abdel-Hafiez, B. Zhang, *Chem. Phys.* **342**, 119 (2007).

[11] R.S. Mulliken, *Phys. Rev.* **36**, 1440 (1930).

[12] D. Zhang, A. Abdel-Hafiez, B. Zhang, *Chin. J. Chem. Phys.* **21**, 12 (2008).

[13] J.G. McCaffrey, H. Kunz, N. Schwentner, *J. Chem. Phys.* **96**, 2825 (1992).

[14] M.C. Heaven, *Chem. Soc. Rev.* **15**, 405 (1986).

[15] D. Maric, J.P. Burrows, *J. Phys. Chem.* **100**, 8645 (1996).

[16] S. Hubinger, J.B. Nee, *J. Photochem. Photobiol. A* **86**, 1 (1995).

[17] M.S. Child, R.B. Bernstein, *J. Chem. Phys.* **59**, 5916 (1973).

[18] J.A. Coxon, *J. Mol. Spectrosc.* **50**, 142 (1974).

[19] D. Zhang, *Polish J. Chem.* **83**, 153 (2009).

[20] E. Wrede, S. Laubach, S. Schulenburg, A. Brown, E.R. Wouters, A.J. Orr-Ewing, M.N.R. Ashfold, *J. Chem. Phys.* **114**, 2629 (2001).

[21] M.J. Cooper, P.J. Jackson, L.J. Rogers, A.J. Orr--Ewing, M.N.R. Ashfold, B.J. Whitaker, *J. Chem. Phys.* **109**, 4367 (1998).

[22] D. Zhang, *J. Math. Chem.* **46**, 576 (2009).

[23] G.E. Hall, P.L. Houston, *Ann. Rev. Phys. Chem.* **40**, 375 (1989).

[24] N. Moiseyev, *Phys. Rep.* **302**, 211 (1998).

[25] R.S. Mulliken, *Phys. Rev.* **50**, 1017 (1936).

[26] D.J. Seery, D. Britton, *J. Phys. Chem.* **68**, 2263 (1964).

[27] D. Zhang, *J. Math. Chem.* **47**, 29 (2010).

[28] A.S. Bracker, E.R. Wouters, A.G. Suits, Y.T. Lee, O.S. Vasyutinskii, *Phys. Rev. Lett.* **80**, 1626 (1998).

[29] A.T.J.B. Eppink, D.H. Parker, *J. Chem. Phys.* **109**, 4758 (1998).

[30] R.N. Zare, *Mol. Photochem.* **4**, 1 (1972).

[31] F.G. Codwin, C. Paterson, P.A. Gorry, *Mol. Phys.* **61**, 827 (1987).

[32] N. Knoblauch, A. Strobel, I. Fischer, V.E. Bondybey, *J. Chem. Phys.* **103**, 5417 (1995).